Formation of C_{60} dimers: A theoretical study of electronic structure and optical absorption

Jan Fagerström and Sven Stafström
Department of Physics and Measurement Technology, Institutionen för Fysik och Mätteknik, Linköping University, S-581 83, Linköping, Sweden

(Received 20 October 1995; revised manuscript received 21 December 1995)

The polymerization of solid C_{60} is studied theoretically within a semi-empirical quantum chemical framework. Model systems consisting of two interacting C_{60} molecules are used in order to model polymerization of neutral C_{60}, as well as of alkali metal doped C_{60}. The geometries and electronic structures of the systems are obtained from semiempirical, AM1, calculations. It is found that the charged systems have a substantially lower energy barrier toward formation of C_{60} dimers, a result in agreement with experiment. This effect is explained in terms of the occupation of bonding intermolecular orbitals as extra charge is added. The reduction of the energy barrier in the case of photopolymerization is motivated in a similar way by promotion of electrons from antibonding, or to bonding, orbitals in the excited state. Furthermore, optical absorption spectra of the neutral and doubly charged C_{60} dimers are calculated from the spectroscopic parametrization of the semiempirical intermediate neglect of differential overlap (INDO) Hamiltonian combined with single excited configuration interaction. The absorption spectrum of the neutral dimer displays distinct peaks with energies and oscillator strengths in qualitative agreement with experiment. Charging of the C_{60} dimer leads to characteristic polarized transitions at low energies. [S0163-1829(96)01919-4]

I. INTRODUCTION

One fascinating group of compounds based on fullerenes consists of the so called fulleride polymers. The existence of such polymers was first realized by Rao *et al.*[1] They discovered that fcc C_{60} films irradiated with visible or ultraviolet light transform to polymer segments with up to 20 covalently bonded C_{60} molecules. They also speculated about the C_{60} molecules binding via [2+2] cycloaddition, although this seemed to contradict x-ray diffraction results in Ref. 1. However, the [2+2]-cycloaddition hypothesis has later been confirmed by several authors, both theoretically[2–5] and experimentally.[6] Subsequent to the discovery of photopolymerized fulleride polymers, it has been found that the same type of polymer structure can be obtained from fcc C_{60} samples via at least two routes: (a) alkali metal doping combined with slow cooling from approximately 500 K to room temperature,[7–10] and (b) hydrostatic pressure treatment at 5 GPa and temperature 800 °C.[11]

The fullerides, i.e., the group of materials based on C_{60} molecules and to which the fulleride polymers belong, display a complicated behavior, with several phase transitions within the temperature range between 0 K and 1000 K. For instance, in the alkali fullerides AC_{60} (where A=K, Rb, or Cs), at least five different phases are believed to exist:[12] spin density wave,[7,13] two different fcc phases [fcc(I) (Ref. 14) and fcc rock salt structure[15]], a ''quenched'' phase consisting of $(AC_{60})_2$ dimers,[16,17] and the alkali fulleride polymer phase.[7–10] In addition, properties of the phases vary substantially depending on the alkali metal used.[13] Various measurements indicate that the alkali fulleride polymer phase has metallic properties.[7,13,18] However, in contrast to the intuitive picture of fulleride polymers as quasi-one-dimensional materials, it is likely that the charge transport is hindered along the chains[19] and instead occurs perpendicular to the axes of the fulleride polymer chains. It is thus clear that fullerides and, as a particular example of this group of materials, fulleride polymers have many properties of fundamental theoretical interest.

In this work, we focus on the question why doped C_{60} in the rocksalt structure tend to polymerize spontaneously, while the undoped material has to be photoexcited or treated at high pressure to polymerize. In order to answer this question, we have studied the electronic structure and optical absorption of a model dimer system consisting of two C_{60} molecules at variable interfullerene distance. Section II explains the methodology used in this study and the results are presented and discussed in Sec. III.

II. METHODOLOGY

In order to model the polymerization, a system of two C_{60} molecules at variable interfullerene distance was used, as schematically displayed in Fig. 1. When R in Fig. 1 becomes small enough, the interfullerene bond is a [2+2] cycloadduct. Photoinduced, as well as doping induced polymerization, was modeled by performing the calculations on a neutral C_{60} pair [denoted $(C_{60})_2$ in this study], as well as on C_{60} pairs with two and six additional electrons [denoted

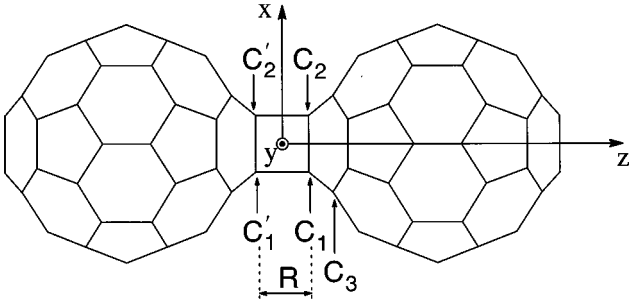

FIG. 1. The C_{60} dimer used in this study as a model for the C_{60} polymer.

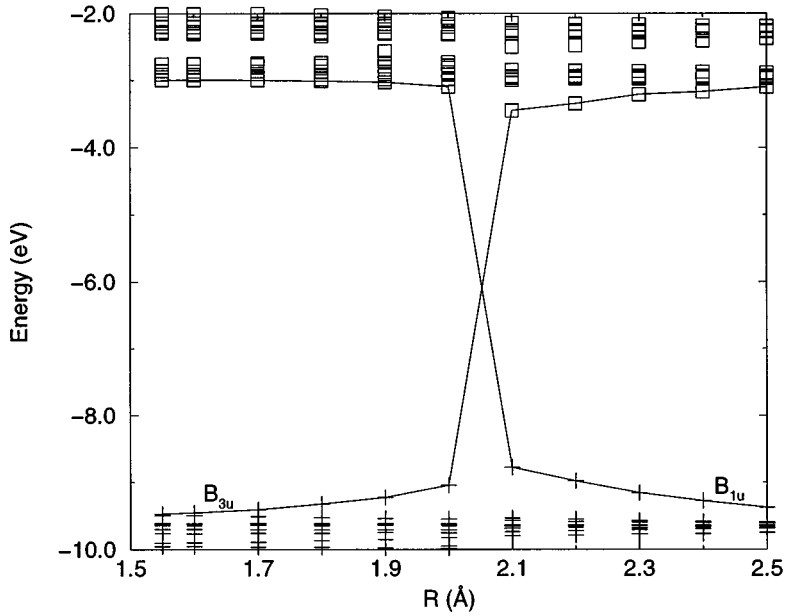

FIG. 2. Correlation diagram of occupied (+) and virtual (□) molecular orbitals for the $(C_{60})_2$ model system, as obtained by the AM1 method.

$(C_{60})_2^{2-}$ and $(C_{60})_2^{6-}$, respectively]. The ionic systems are models for AC_{60} and A_3C_{60}, where A is an alkali metal atom. The intermolecular distance R was decreased from 2.5 Å to the equilibrium bond length (approximately 1.5 Å, as obtained in the geometry optimization calculations) in steps of 0.10 Å. At each step, the geometry, electronic structure and total energy were obtained self-consistently within the restricted Hartree-Fock method by use of the Austin model 1 (AM1) (Ref. 20) Hamiltonian. All atomic coordinates were left unconstrained during the geometry optimization, except those describing the positions of the four atoms in the [2+2] cycloadduct (C_1, C_1', C_2, and C_2' in Fig. 1). The coordinates of these four atoms were restricted to vary only within the xz plane (see Fig. 1) for the structures at equilibrium bond lengths, and only along the x axis for the other structures.

In order to monitor the change of individual molecular orbitals as a function of the interfullerene distance R, it was necessary to study the molecular orbital symmetries. The ideal C_{60} molecule belongs to the icosahedral symmetry point group I_h. Two C_{60} molecules, bonded via [2+2] cycloaddition, thus constitute a system with D_{2h} symmetry. In the present calculations, however, no symmetry restriction was imposed upon the molecular geometries. Hence, the optimized geometries are not fully (although very closely) D_{2h} symmetrical, and the molecular orbitals obtained by the geometry optimization calculations do not exactly correspond to representations of the D_{2h} point group. This fact made it impossible to determine the symmetry of some molecular orbitals. However, most orbitals close to the highest occupied molecular orbital (HOMO) and lowest unoccupied molecular orbital (LUMO) could unambiguously be symme-

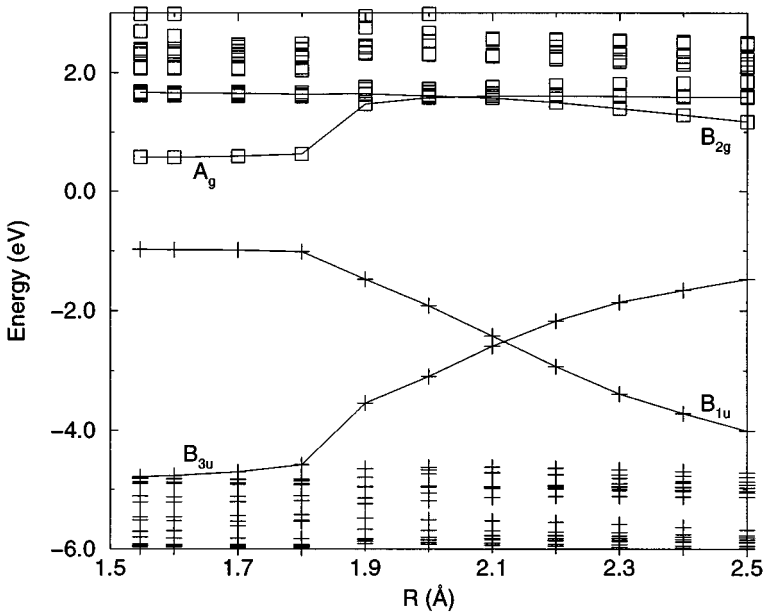

FIG. 3. Same as Fig. 2, but for the $(C_{60})_2^{2-}$ model system.

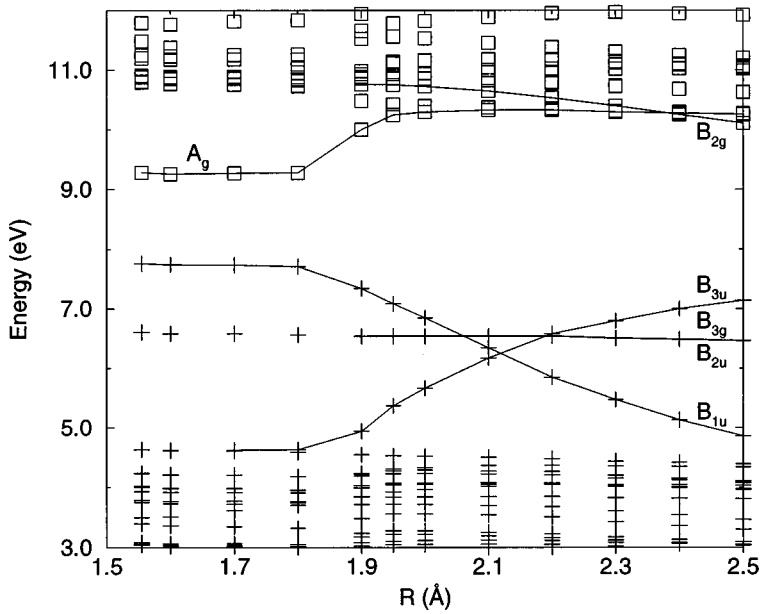

FIG. 4. Same as Fig. 2, but for the $(C_{60})_2^{6-}$ model system.

try classified by inspection of the graphical representations of the orbitals. The symmetries thus obtained are the basis of the correlation diagrams of molecular orbitals in Sec. III, Figs. 2, 3, and 4. (The correlations in Figs. 2, 3, and 4 are only indicated for those molecular orbitals, which are relevant to this study.)

Optical absorption spectra of the different systems were calculated using the INDO/1 spectroscopic parametrization[21] of the semiempirical intermediate neglect of differential overlap (INDO) Hamiltonian,[22] combined with single excited configuration interaction (SCI). This method has previously been successfully applied to C_{60} (Ref. 23). The configurations were generated from an active space consisting of molecular orbitals number 121–360. For instance, for $(C_{60})_2$, where the HOMO is molecular orbital number 240, the active space consisted of 120 occupied and 120 virtual orbitals. The oscillator strengths of the transitions from ground state (i.e., the Hartree-Fock determinant) to the excited CI wave functions were calculated in the length gauge as

$$f_{\rm osc}=\frac{2m_e(E_{\rm SE}-E_{\rm HF})}{3\hbar^2}\left|\left\langle {\rm HF}\left|\sum_{i=1}^{N_{\rm el}}\mathbf{r}_i\right|{\rm SE}\right\rangle\right|^2, \qquad (1)$$

where m_e is the electronic mass, $\hbar$ is Planck's constant, $|{\rm HF}\rangle$, $|{\rm SE}\rangle$, $E_{\rm HF}$, and $E_{\rm SE}$ are the Hartree-Fock and single excited CI wave functions and energies, respectively, $N_{\rm el}$ is the number of electrons and $\mathbf{r}_i$ is the position operator of electron i. To simulate broadening, due to vibrations and interaction with surrounding molecules, etc., each transition was broadened using a Gaussian function with full width at half maximum (FWHM) equal to 0.2 eV. The resulting Gaussian curves were finally added to obtain the total absorption spectrum.

III. RESULTS AND DISCUSSION

The bond lengths close to the [2+2] cycloadduct, as obtained by geometry optimization of the three model systems in this study, are summarized in Table I. Corresponding values from the experimental study in Ref. 10 are also listed. The experimental bond lengths for AC_{60} (A=Rb or K) were extracted from x-ray powder diffraction data and correspond to the theoretical results for $(C_{60})_2^{2-}$ in the present study. The experimental C_1–C_3 bond lengths of 1.50 and 1.51 Å, respectively, agree very well with our calculated value 1.52 Å. For the interfullerene bond C_1–C_1', the theoretical value 1.55 Å falls between the experimental values 1.44 Å and 1.65 Å and within estimated experimental errors. Finally, the experimental value of the intra-Fullerene bond C_1–C_2 is up to 0.30 Å larger than the theoretical result.

The spread in the experimental values for the C_1–C_1' and C_1–C_2 bond lengths (see Table I) indicates that the counterion has some influence on the geometries of the polyanions. However, it is difficult to judge exactly how the counterions affect the bond lengths. There is no obvious trend in the limited data of Table I and we have no means of including alkali metal atoms of different kinds within the AM1 method.

A striking feature of the theoretical results in Table I is that the charge of the system has a very small effect on the geometrical structure of the [2+2] adduct. This is a result of the charge distribution, namely, a tendency of the excess electrons to localize away from the intermolecular bonding sites. This point will be discussed in more detail below.

The change in total energy as the interfullerene bond lengths decrease is shown in Fig. 5 for all three model systems, $(C_{60})_2$, $(C_{60})_2^{2-}$, and $(C_{60})_2^{6-}$. All curves have been shifted to the same reference total energy at R=2.5 Å, in order to simplify comparison between the different systems. The most striking feature of Fig. 5 is the large differences in the height of the energy barriers between the neutral system and the two charged model systems. The energy barrier of $(C_{60})_2^{2-}$ is only approximately one fifth of that of the neutral dimer. This result is in qualitative agreement with experiments, which show that alkali metal doped C_{60} films polymerize spontaneously[7,10] below a certain transition tempera-

TABLE I. Bond lengths (in Å) at the [2+2] cycloadduct for the three model systems $(C_{60})_2$, $(C_{60})_2^{2-}$, and $(C_{60})_2^{6-}$. Notations of bonds refer to Fig. 1.

System	Method	C_1–C_2 [a]	C_1–C_1' [b]	C_1–C_3
$(C_{60})_2$	AM1 (This study)	1.61	1.55	1.52
$(C_{60})_2^{2-}$	AM1 (This study)	1.60	1.55	1.52
RbC_{60}	Experiment [c]	1.90 ± 0.15	1.44 ± 0.15	1.51 ± 0.15
KC_{60}	Experiment [d]	1.74 ± 0.20	1.65 ± 0.20	1.50 ± 0.20
$(C_{60})_2^{6-}$	AM1 (This study)	1.61	1.55	1.52

[a]Same as $C_1'-C_2'$.
[b]Same as C_2-C_2'.
[c]With Rb counterions. Experimental results obtained from Rietveld fits to powder x-ray diffraction spectra, see Ref. 10.
[d]With *K* counterions. Experimental results obtained from Rietveld fits to powder x-ray diffraction spectra, see Ref. 10.

ture, while pristine C_{60} only polymerize upon irradiation of visible/UV radiation[1] or when treated with high pressure.[11]

Experimentally the heat of transformation from the RbC_{60} polymer phase to the rocksalt structure has been measured by differential scanning calorimetry to 32 J/g.[14] With the estimated rotational contribution subtracted, this value is reduced to 25.4 J/g. Assuming that the number of interfullerene bonds in the polymers in this measurement were approximately the same as the number of RbC_{60} units (i.e., the length of the polymers was much greater than two monomers) this yields 0.21 eV/bond. This is less than one sixth of 1.44 eV, which is the calculated energy difference between $R=2.5$ and equilibrium bond length for $(C_{60})_2^{2-}$ (see Fig. 5).

In the case of phototransformed C_{60} polymers, Wang *et al.*[24] have measured the activation energy E_a needed to separate photogenerated C_{60} dimers and found $E_a=1.25$ eV. This value should be compared with the energy difference of 3.5 eV for $(C_{60})_2$ between the top of the energy barrier in Fig. 5 and the energy at equilibrium bond length. Again, the calculated value is too large as compared with experiment.

It is difficult to fully rationalize the discrepancy between theory and experiment regarding the binding energy and the height of the energy barrier. However, there are some factors not accounted for in the present calculation, which might influence the polymerization energetics to some extent. For instance, surrounding molecules or polymer chains can affect the dimerization by putting geometrical constraints on the reaction. It should be noted that the polymers used in the experimental studies above were obtained by polymerizing crystalline C_{60}, a process which introduces some strain in the sample. In the case of doping induced polymerization, the Coulomb potential of the positive counterions might also have some influence on the dimer formation energies. From the theoretical methodology point of view, it is clear that calculations of total energies of C_{60} dimers are rather sensitive to the choice of method. Values of the total energy difference between two separate C_{60} molecules compared to the bound $(C_{60})_2$ dimer have been obtained in the range from -0.60 eV to 2.1 eV (Refs. 2–5), using molecular dynamics, semiempirical methods, as well as *ab initio* calculations. The corresponding (semiempirical) value in the present study is 1.42 eV. Because of the reasons mentioned here, one should be careful not to make any conclusions from the absolute values of the energy barrier height or from the slight difference in energy barrier between $(C_{60})_2^{2-}$ and $(C_{60})_2^{6-}$. It should be stressed, however, that the discrepancy between theory and experiment does not affect the conclusion that $(C_{60})_2$ has a substantially larger dimerization energy barrier than the two charged model systems. This point is also clarified in the discussion below.

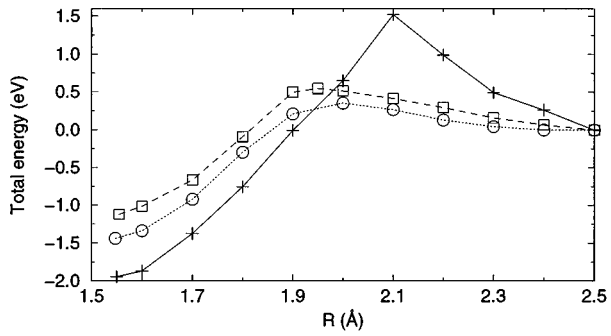

FIG. 5. Calculated total energies for $(C_{60})_2$ (+), $(C_{60})_2^{2-}$ (○), and $(C_{60})_2^{6-}$ (□). The curves have been shifted to zero total energy at $R=2.5$ Å.

The total energy calculations on $(C_{60})_2^{6-}$ suggest that A_3C_{60} polymerize spontaneously, just as AC_{60} (see Fig. 5). However, to the best of our knowledge, this has never been observed experimentally. It might be the case that the polymerization is hindered by the counterions in A_3C_{60} or that other geometrical constraints force the molecules to stay apart. To ultimately answer this question, it would be necessary to include at least counterions and preferably also increase the number of C_{60} molecules in the model system.

Why does the dimerization energy barrier more or less disappear upon doping? The answer can be found in Figs. 2, 3, and 4 which show the correlation of molecular orbitals for $(C_{60})_2$, $(C_{60})_2^{2-}$, and $(C_{60})_2^{6-}$ as a function of the interFullerene bond length. Study Fig. 2 which corresponds to $(C_{60})_2$. At $R=2.5$ Å, the spectrum is seen to approach the molecular orbital spectrum of two separated C_{60} molecules, e.g., the twelve orbitals in the lowest part of the unoccupied spectrum are grouped six by six and correspond to the threefold degenerate t_{1u} and the t_{1g} levels of two C_{60} molecules. Similarly, the ten topmost occupied molecular orbitals correspond to the fivefold degenerate h_u-levels in C_{60}. The HOMO at $R=2.5$ Å is antibonding with respect to the xy

plane (see Fig. 1) and of B_{1u} symmetry. The LUMO, however, which has B_{3u} symmetry, is bonding. As a consequence, when R is decreased from 2.5 Å, the B_{1u} energy increases and the B_{3u} energy decreases. When R is small enough, somewhere between 2.1 Å and 2.0 Å, the two levels cross. This means that the HOMO of $(C_{60})_2$ is antibonding for $R \geq 2.1$ Å, but bonding for $R \leq 2.0$ Å. The behavior of the total energy curve for $(C_{60})_2$ in Fig. 5 reflects this behaviour of the HOMO in Fig. 2. Thus, there is a barrier in the total energy, which peaks close to the crossing of the bonding B_{3u} and the antibonding B_{1u} levels. (Note that the energy separation between the HOMO and the LUMO is very large as a result of the Hartree-Fock method.)

With the molecular orbital diagram in Fig. 2 the photopolymerization can be explained as follows. When an undoped C_{60} film in the fcc phase is exposed to visible/UV light, an electron from the B_{1u} level (at $R > 2.5$ Å) is promoted to some of the unoccupied orbitals. This results in a depopulation of the antibonding B_{1u} level and thus a strengthening of the intermolecular bond. Alternatively, electrons can be promoted from molecular orbitals below the HOMO to the bonding B_{3u} level, resulting in a similar situation as for doped C_{60}. Excitations from B_{1u} to B_{3u} are dipole forbidden and do consequently not contribute to the photopolymerization process.

A similar kind of reasoning as that used for $(C_{60})_2$ can be applied to the charged model systems in Figs. 3 and 4, with the important difference compared to the neutral case that both the bonding B_{3u} and the antibonding B_{1u} levels are occupied. Thus, *the energy variation of these molecular orbitals with changing R tend to cancel, which results in a lower total energy barrier as compared to the neutral case.* The driving mechanism for polymerization is thus of slightly different origin in the case of doping-induced polymerization, as compared to photoinduced polymerization. When the material is doped, the interfullerene bond is strengthened, due to the occupation of the bonding B_{3u} level; when the material is photoexcited, the interfullerene bond is strengthened due to the deoccupation of the antibonding B_{1u} level and due to occupation of the bonding B_{3u} level by electrons from orbitals below the HOMO.

It is clear that variation of the total energy is not exclusively accounted for by the B_{1u} and B_{3u} levels, since the total energy curve varies even for the charged systems, especially for R close to equilibrium bond length. The explanation for this is at least twofold. First, the Hartree-Fock total energy is not simply the sum of molecular orbital energies, but also includes Coulomb and exchange interaction between electrons in different molecular orbitals. It is, therefore, difficult to exactly tell how much the total energy will be affected by a certain change in energy of one molecular orbital. Second, there are 478 electrons in 239 molecular orbitals below the HOMO of $(C_{60})_2$, which all contribute to the total energy. Small changes in many of these low-lying orbitals can have a large influence on the total energy. For instance, the rather large stabilization for all three model systems below $R = 1.9$ Å must, to a large extent, be accounted for by changes in low-lying orbitals. Nevertheless, it is likely that the complementary behavior of the B_{1u} and B_{3u} levels is the single most important factor that determines whether the fullerenes will bind spontaneously or not.

The striking similarities in the geometrical structure around the [2+2] cycloadduct for all three systems included in this study (see Table I) can also be explained by inspection of the molecular orbitals. The major difference in the correlation diagrams (Figs. 2–4) between the neutral system and the two anionic systems is that, at equilibrium bond length, the B_{1u} orbital is unoccupied in the neutral case, but occupied in the other two cases. Clearly, in order for the geometry around the [2+2] cycloadduct to remain unchanged upon occupation of the B_{1u} orbital, it is expected that this orbital is localized to other parts of the dimer. This is indeed the case. Inspection of the molecular orbital coefficients shows that the B_{1u} orbital is nonbonding in the C_1–C_1', C_1–C_2, and C_1–C_3 bonds. (Thus, the character of the B_{1u} level changes from antibonding at $R = 2.5$ Å to nonbonding at equilibrium bond length.) This result connects closely to a previous study of the C_{60} polyanion,[19] which showed that the highest occupied band in this system is dispersionless for exactly the same reason as discussed here, namely, the nonbonding character of these orbitals at the sites of the intermolecular interaction unit.

We now turn to the calculations of optical absorption spectra. In order to utilize symmetry to reduce the size of the CI problem, all geometries used in the CI calculations were restricted to the D_{2h} point group, during the AM1 geometry optimization. The active space used in the calculations of the spectra, 120 occupied and 120 virtual orbitals in the case of $(C_{60})_2$, was chosen on the basis of several test calculations with different active spaces and the restriction that maximum 2000 configurations could be used for each irreducible representation of D_{2h}. It turns out that mixing of configurations with relatively high energies [where electrons are promoted from (to) molecular orbitals far from the HOMO (LUMO)] is strong even for CI wave functions with energies closest to the ground state. It is, therefore, essential to include such configurations if a converged spectrum is desired, i.e., a spectrum which is basically unaffected by further increase of the active space. In fact, it is easy to be mislead by using a minimal active space of, e.g., 28 occupied and 12 virtual orbitals (which corresponds to the g_g, h_g, h_u, t_{1u}, and t_{1g} levels closest to the HOMO-LUMO levels in the C_{60} molecule). Such a minimal active space leads to a SCI optical absorption spectrum, which resembles the experimental spectrum quite closely. However, if the active space is slightly increased, most of the resemblance is lost.[25]

Inclusion of doubly (and higher) excited configurations in the CI would not affect the present SCI spectra in any substantial way. This could be concluded by comparing SCI results with calculations performed within the random phase approximation (RPA) (Refs. 26 and 27), using the same active space.[25] Doubly excited determinants are included in RPA calulations,[28] although in a different way than in CI.

Figure 6 displays the optical absorption of $(C_{60})_2$ at equilibrium bond length. The impulses indicate the energies and oscillator strengths of the individual excitations. The individual excitations have been broadened with a Gaussian distribution (FWHM = 0.2 eV) and the resulting curves have been added at each energy to obtain the absorption spectrum. There is a large amount of allowed transitions densely distributed above approximately 3 eV. A general feature of the spectrum in Fig. 6 is the increase of the oscillator strength up

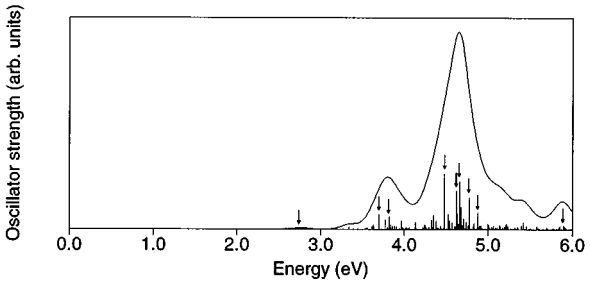

FIG. 6. Optical absorption spectrum, as obtained by the INDO/1 SCI method applied to $(C_{60})_2$ at equilibrium interfullerene bond length ($R=1.548$ Å). The active space contained 120 occupied and 120 virtual molecular orbitals. The energies and oscillator strengths of individual transitions are indicated by the impulses. The spectrum has been broadened using Gaussian functions, with FWHM$=0.2$ eV.

to approximately 4.5 eV, where the oscillator strengths start to decrease. There are assemblies of important transitions at approximately 2.7 eV, 3.7–3.8 eV, 4.5–4.9 eV, and 5.9 eV, which give rise to the four distinct peaks in the broadened absorption spectrum. Qualitatively, the same behavior has been observed experimentally[29] in optical absorption measurements of photopolymerized C_{60} films. In that case, four main peaks were observed below 6 eV at 2.7, 3.7, 4.8, and 5.7 eV.

In order to get an impression of the character of the different transitions in the spectrum in Fig. 6, the CI wave functions of the excited states involved in some of the most important transitions are listed in Table II. The wave functions correspond to the transitions that are marked with arrows in Fig. 6. As mentioned above, the mixing of different configurations is very strong. This can be concluded from Table II by noting that although there are only quite few configurations listed for each transition, the coefficients are still rather small. Using an analogy to the C_{60} Hückel molecular orbital spectrum, it was argued in Ref. 29 that the experimentally observed transition at 2.7 eV was due to the promotion of electrons from the **HOMO-1** levels (boldface indicates that **HOMO-1** refers to a group of orbitals, namely, levels in the polymer derived from the C_{60} g_g and h_g orbitals) to the **LUMO** levels (derived from the C_{60} t_{1u} orbitals) or from the **HOMO** levels (derived from the C_{60} h_u orbitals) to the **LUMO+1** levels (derived from the C_{60} t_{1g} orbitals). That picture has to be slightly modified by the present results. The transition at 2.749 eV contains configurations with electrons promoted from **HOMO** [molecular orbitals 231–240 for $(C_{60})_2$] to **LUMO** (orbitals 241–246), **LUMO+1** (orbitals 247–252), as well as to **LUMO+2** (orbitals 253–262). Similarly, the experimentally observed transition at 3.7 eV was pictured as promotion of electrons from **HOMO-1** to **LUMO+1**. In contrast, the transitions at 3.695 eV and 3.821 eV in Table II are dominated by configurations in which electrons are promoted from **HOMO** to **LUMO**, **LUMO+1**, and **LUMO+2**.

The experimental spectra in Ref. 29 show that the positions of the four main peaks are largely unaffected by the polymerization process, apart from a shift of 0.1 eV for the three upper peaks, which appear at 3.6 eV, 4.7 eV, and 5.6 eV in the case of pristine solid C_{60}. To make a comparison with unpolymerized C_{60} within the present model, the theoretical spectrum of a single C_{60} molecule is shown in Fig. 7 and the corresponding CI wave functions are displayed in Table III. The geometry of the C_{60} molecule was restricted to D_{2h} symmetry and was obtained by the AM1 method. An active space of 60 occupied and 60 virtual molecular orbitals was used in the calculation. Further increase of the active space does not substantially change the spectrum.[23] The spectrum in Fig. 7 agrees excellently with optical absorption measurements of C_{60} in solution.[30] The theoretical spectrum

TABLE II. Selected transitions (marked with arrows in Fig. 6) from the INDO/1 SCI results for D_{2h}-symmetric neutral dimer $(C_{60})_2$ at equilibrium interfullerene bond length (R$=1.548$ Å). The active space included molecular orbitals 121–360. Only configurations that contribute more than 5% (i.e., with squared CI coefficients greater than 0.05) are listed. ''Final state'' denotes the state to which the transition takes place. (State 1 is the ground state.)

Final state	Energy (eV)	Osc. strength [a]	Ψ_{CI}
30	2.749	0.034 (z)	$-0.311\|234\rightarrow248\rangle+0.273\|235\rightarrow250\rangle$
			$-0.261\|238\rightarrow254\rangle-0.240\|240\rightarrow245\rangle$
			$+0.330\|231\rightarrow259\rangle+0.326\|232\rightarrow257\rangle$
119	3.695	0.642 (z)	$+0.295\|238\rightarrow246\rangle-0.249\|239\rightarrow261\rangle$
			$+0.285\|240\rightarrow252\rangle$
144	3.821	0.542 (x)	$+0.519\|234\rightarrow244\rangle-0.445\|235\rightarrow243\rangle$
			$-0.233\|239\rightarrow253\rangle$
321	4.478	2.366 (z)	$+0.237\|228\rightarrow243\rangle+0.244\|230\rightarrow258\rangle$
354	4.623	1.647 (y)	No single configuration contributes more than 5%
366	4.660	2.030 (x)	$+0.273\|224\rightarrow252\rangle+0.273\|226\rightarrow254\rangle$
410	4.776	1.350 (y)	$-0.231\|225\rightarrow247\rangle+0.225\|228\rightarrow249\rangle$
442	4.878	0.710 (x)	$-0.248\|217\rightarrow247\rangle-0.225\|224\rightarrow252\rangle$
			$-0.271\|235\rightarrow255\rangle+0.334\|238\rightarrow259\rangle$
860	5.894	0.168 (y)	$+0.327\|220\rightarrow270\rangle+0.325\|221\rightarrow273\rangle$

[a] x, y, and z indicate the polarization direction of the transition in the coordinate system of Fig. 1.

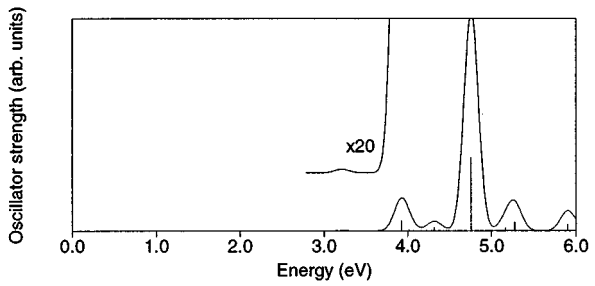

FIG. 7. Same as Fig. 6, but for C_{60}. The active space contained 60 occupied and 60 virtual molecular orbitals.

in Fig. 7 also agrees qualitatively with experimental measurements on solid pristine C_{60} (Ref. 29) in the sense that it displays major peaks a few tenths of electron volts below 4, 5, and 6 eV and the oscillator strength is largest for the transitions at 4.757 eV. However, the peaks at 3.923 eV, 4.757 eV, and 5.903 eV appear at slightly too high energies. Furthermore, the major peaks are down shifted by approximately 0.1 eV, in the calculated spectrum of $(C_{60})_2$ (Fig. 6), as compared to the calculated spectrum of C_{60} (Fig. 7). This is in contrast to the slight upshift, which is observed experimentally for C_{60} in the polymer phase, as compared to C_{60} in the pristine solid phase.[29] It should also be noted that the peak at 5.273 eV has no counterpart in the experimental spectrum of solid C_{60} and that the experimentally observed peak at 2.7 eV is not obtained in the SCI calculation. Instead there is a weak threefold degenerate transition at 3.213 eV. These discrepancies must obviously be accounted for by effects that are not included in the present model. It is likely that, e.g., screening of the Coulomb interaction will modify the absorption spectra, an effect which has been observed in similar studies of conjugated polymers.[31] It must be stressed, however, that the general agreement between theory and experiment is good and the present calculation is probably a quite accurate description of the processes involved in the polymerization. In particular, it is convincing that, in spite of the strong mixing of different configurations and the large number of transitions in the case of $(C_{60})_2$, the main peaks appear at the correct energies with qualitatively the correct oscillator strengths. Note that many of the $(C_{60})_2$ transitions in Fig. 6 contain contributions not only from the corresponding C_{60} peaks, but also mix with other types of configurations. For instance, using the nomenclature described above, the transitions between 4.478 eV and 4.878 eV in Table II contain many configurations with electrons promoted from **HOMO-1** to **LUMO+1**. The corresponding transitions at 4.756 eV and 4.757 eV in Table III lack this type of configurations.

The optical absorption spectrum and corresponding CI wave functions for $(C_{60})_2^{2-}$ are shown in Fig. 8 and Table IV. In the energy range above 3 eV, the absorption spectra of $(C_{60})_2^{2-}$ and $(C_{60})_2$ are qualitatively the same. The peaks are less distinct for the charged system and a notable structure within the peaks emerge. From the eigenenergy spectrum of the molecular orbitals at equilibrium bond lengths, displayed on the left hand side of Figs. 2 and 3, it is evident that transitions, which are dominated by electron excitations that do not involve the HOMO and LUMO levels, are basically unaffected by the extra charges in $(C_{60})_2^{2-}$. However, as discussed above, the extra charges have a major effect on the HOMO and the LUMO. Consequently, peaks induced by the extra charges appear in the optical absorption spectrum, which are dominated by configurations in the CI wave function where electrons have been promoted from the HOMO and/or to the LUMO levels. These peaks appear at 0.60 eV, and at approximately 1 eV and 1.5 eV. It should be noted that the peak at 0.60 eV is completely dominated by the CI configuration, where an electron has been promoted from the HOMO to the LUMO. The symmetries of the HOMO and the LUMO (B_{1u} and A_g, respectively) imply a transition polarized in the z direction, i.e., the direction of the polymer. Thus, the symmetries of the HOMO and the LUMO of the doped C_{60} polymer are manifested in the optical absorption spectrum, as a distinct peak at low energy with polarization in the direction of the polymer. Although it is possible that there are transitions at similar energies in doped, but unpolymerized C_{60}, these transition are not likely to be polarized in the z direction, since the HOMO change irreducible representation at $R=2.1$ Å, due to the crossing discussed above. In fact, optical transitions in unpolymerized solid C_{60} are not expected to be polarized at all, since the C_{60} molecules have been observed to be in rapid rotational motion at room temperature.[32]

It has been observed that polymerized KC_{60} is transparent to visible light.[9] The absorption spectrum in Fig. 8 is in excellent agreement with this observation. Visible light falls in the energy range 1.6–3.1 eV, where the absorption is very limited in the calculated spectrum.

IV. SUMMARY AND CONCLUSIONS

Three different C_{60} dimer systems, with zero, two, and six electrons added, have been studied theoretically in order to model photoinduced and doping-induced polymerization of C_{60}. In agreement with experiment, the energy barrier in the dimer formation process is large for neutral $(C_{60})_2$, and disappear almost totally in $(C_{60})_2^{2-}$ and $(C_{60})_2^{6-}$. This effect is explained by the character of the HOMO and the LUMO in $(C_{60})_2$. At large interfullerene distances, the HOMO in $(C_{60})_2$ is antibonding and, therefore, tends to increase the energy of the system as the interfullerene bond length decreases. However, occupation of the LUMO of $(C_{60})_2$, which is a bonding molecular orbital at large interfullerene distances, tends to compenstate this energy increase, leading

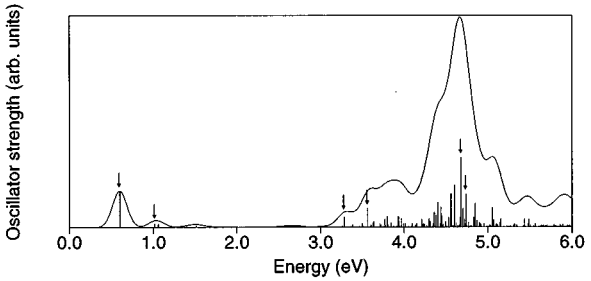

FIG. 8. Same as Fig. 6, but for $(C_{60})_2^{2-}$ with $R=1.546$ Å. The active space contained 121 occupied and 119 virtual molecular orbitals.

TABLE III. Selected transitions from the INDO/1 SCI results for D_{2h}-symmetric neutral C_{60}. The active space included molecular orbitals 61–180. Only configurations that contribute more than 5% (i.e., with squared CI coefficients greater than 0.05) are listed. ''Final state'' denotes the state to which the transition takes place. (State 1 is the ground state.)

Final state	Energy (eV)	Osc. strength	Ψ_{CI}
11	3.213	0.003 (z)	$-0.369\|116\rightarrow132\rangle-0.296\|117\rightarrow126\rangle$
			$-0.227\|117\rightarrow132\rangle-0.298\|118\rightarrow124\rangle$
			$-0.298\|119\rightarrow125\rangle+0.309\|120\rightarrow133\rangle$
			$-0.300\|120\rightarrow134\rangle$
12	3.213	0.003 (x)	$+0.347\|116\rightarrow124\rangle+0.435\|117\rightarrow130\rangle$
			$+0.298\|118\rightarrow126\rangle-0.414\|119\rightarrow133\rangle$
			$-0.298\|120\rightarrow125\rangle$
13	3.213	0.003 (y)	$-0.382\|116\rightarrow131\rangle+0.305\|117\rightarrow125\rangle$
			$-0.417\|118\rightarrow134\rangle-0.298\|119\rightarrow126\rangle$
			$+0.298\|120\rightarrow124\rangle$
29	3.922	0.531 (x)	$-0.485\|116\rightarrow124\rangle+0.225\|117\rightarrow130\rangle$
			$-0.424\|118\rightarrow126\rangle+0.428\|120\rightarrow125\rangle$
30	3.923	0.529 (z)	$+0.252\|116\rightarrow126\rangle-0.415\|117\rightarrow126\rangle$
			$-0.426\|118\rightarrow124\rangle-0.425\|119\rightarrow125\rangle$
31	3.923	0.529 (y)	$+0.233\|116\rightarrow125\rangle+0.425\|117\rightarrow125\rangle$
			$-0.427\|119\rightarrow126\rangle+0.426\|120\rightarrow124\rangle$
74	4.756	3.783 (z)	$+0.305\|111\rightarrow122\rangle+0.250\|111\rightarrow129\rangle$
			$-0.306\|113\rightarrow121\rangle+0.350\|114\rightarrow123\rangle$
			$+0.266\|116\rightarrow132\rangle-0.224\|120\rightarrow133\rangle$
75	4.757	3.782 (x)	$-0.306\|111\rightarrow123\rangle+0.305\|112\rightarrow121\rangle$
			$-0.250\|112\rightarrow128\rangle-0.323\|115\rightarrow122\rangle$
			$+0.311\|117\rightarrow130\rangle-0.299\|119\rightarrow133\rangle$
76	4.757	3.783 (y)	$-0.305\|112\rightarrow122\rangle-0.305\|113\rightarrow123\rangle$
			$-0.250\|113\rightarrow127\rangle-0.282\|115\rightarrow121\rangle$
			$-0.273\|116\rightarrow131\rangle-0.302\|118\rightarrow134\rangle$
95	5.273	0.443 (x)	$+0.707\|107\rightarrow127\rangle+0.360\|108\rightarrow128\rangle$
			$-0.381\|110\rightarrow129\rangle$
96	5.273	0.447 (y)	$+0.702\|108\rightarrow129\rangle+0.354\|109\rightarrow127\rangle$
			$-0.398\|110\rightarrow128\rangle$
97	5.273	0.444 (z)	$+0.365\|107\rightarrow129\rangle+0.706\|109\rightarrow128\rangle$
			$-0.379\|110\rightarrow127\rangle$
113	5.903	0.343 (z)	$+0.376\|90\rightarrow123\rangle+0.347\|93\rightarrow121\rangle$
			$-0.351\|94\rightarrow122\rangle+0.249\|98\rightarrow124\rangle$
			$-0.250\|100\rightarrow125\rangle+0.265\|102\rightarrow126\rangle$
114	5.903	0.344 (x)	$-0.314\|90\rightarrow122\rangle+0.252\|91\rightarrow122\rangle$
			$+0.351\|92\rightarrow121\rangle-0.349\|94\rightarrow123\rangle$
			$-0.250\|98\rightarrow126\rangle+0.249\|99\rightarrow125\rangle$
			$+0.230\|102\rightarrow124\rangle$
115	5.903	0.340 (y)	$-0.398\|91\rightarrow121\rangle+0.344\|92\rightarrow122\rangle$
			$+0.350\|93\rightarrow123\rangle+0.251\|99\rightarrow124\rangle$
			$+0.248\|100\rightarrow126\rangle-0.283\|101\rightarrow125\rangle$

to substantial reduction of the energy barrier for dimer formation in $(C_{60})_2^{2-}$ and $(C_{60})_2^{6-}$. Photopolymerization is explained by deoccupation of the antibonding HOMO and occupation of the bonding LUMO by electrons from below the HOMO, thus leading to a reduction of the energy barrier.

The theoretically calculated heats of transformation and activation energies for the dimerizations in the present study are systematically too large, as compared to experiments. This discrepancy is difficult to fully explain. The theoretical values are probably improved if strain and Coulomb effects of surrounding molecules and ions are accounted for. It should also be noted that the absoulute values of the dimer binding energies are sensitive to the method used, which is seen by comparison with other theoretical studies.

Calculations of optical absorption spectra for C_{60}, using the SCI method, show general agreement with optical absorption measurements on pristine solid C_{60}. Formation of dimers results in strong mixing of configurations, which leads to a large number of transitions above 3 eV. However, the distribution of transitions is such that four distinct peaks

TABLE IV. Same as Table II, but for $(C_{60})_2^{2-}$ (D_{2h} symmetry) with $R=1.546$ Å. The transitions in the table are indicated with arrows in Fig. 8.

Final state	Energy (eV)	Osc. strength	Ψ_{CI}
4	0.600	1.463 (z)	$-0.980\|241\rightarrow242\rangle$
5	1.017	0.147 (y)	$-0.133\|241\rightarrow243\rangle-0.956\|241\rightarrow247\rangle$
			$+0.107\|241\rightarrow264\rangle$
48	3.285	0.424 (z)	$+0.231\|233\rightarrow265\rangle+0.268\|234\rightarrow263\rangle$
			$-0.233\|235\rightarrow252\rangle-0.230\|236\rightarrow253\rangle$
			$+0.294\|238\rightarrow247\rangle-0.288\|239\rightarrow251\rangle$
			$+0.375\|240\rightarrow248\rangle$
59	3.564	0.759 (z)	$-0.332\|220\rightarrow242\rangle-0.225\|235\rightarrow252\rangle$
			$+0.267\|235\rightarrow265\rangle+0.331\|238\rightarrow264\rangle$
			$-0.291\|239\rightarrow251\rangle+0.237\|240\rightarrow248\rangle$
166	4.681	2.811 (x)	No single configuration contributes more than 5%.
172	4.741	1.335 (y)	$+0.294\|216\rightarrow248\rangle-0.286\|220\rightarrow247\rangle$
			$+0.239\|225\rightarrow250\rangle+0.308\|227\rightarrow253\rangle$

appear at 2.7 eV, 3.8 eV, 4.6 eV, and 5.9 eV, with maximum oscillator strength at the 4.6 eV peak, which conforms well to optical absorption experiments on photopolymerized C_{60}.

The optical absorption spectrum of $(C_{60})_2^{2-}$ contains a peak at 0.60 eV, not seen in the $(C_{60})_2$ spectrum, which is completely dominated by the promotion of an electron from the HOMO to the LUMO of the dianion. This peak is well separated from other major transitions and absorb light which is polarized in the direction of the polymer. The absorption is small in the energy range of visible light, which is in full agreement with experimental observations.

ACKNOWLEDGMENTS

Many thanks to Professor Michael C. Zerner for providing the program used in the present study. Financial support from the Swedish Research Council for Engineering Science (TFR) is gratefully acknowledged.

[1] A. M. Rao *et al.*, Science **259**, 955 (1993).
[2] D. L. Strout *et al.*, Chem. Phys. Lett. **214**, 576 (1993).
[3] M. Menon, K. R. Subbaswamy, and M. Sawtarie, Phys. Rev. B **49**, 13 966 (1994).
[4] N. Matsuzawa, M. Ata, D. A. Dixon, and G. Fitzgerald, J. Phys. Chem. **98**, 2555 (1994).
[5] G. B. Adams, J. B. Page, O. F. Sankey, and M. O'Keeffe, Phys. Rev. B **50**, 17 471 (1994).
[6] P. Zhou, Z.-H. Dong, A. M. Rao, and P. C. Eklund, Chem. Phys. Lett. **211**, 337 (1993).
[7] O. Chauvet *et al.*, Phys. Rev. Lett. **72**, 2721 (1994).
[8] S. Pekker, L. Forró, L. Mihály, and A. Jánossy, Solid State Commun. **90**, 349 (1994).
[9] S. Pekker *et al.*, Science **265**, 1077 (1994).
[10] P. W. Stephens *et al.*, Nature **370**, 636 (1994).
[11] Y. Iwasa *et al.*, Science **264**, 1570 (1994).
[12] P. W. Stephens, in *Physics and Chemistry of Fullerenes and Derivatives* (World Scientific, Singapore, 1995), p. 291.
[13] F. Bommeli *et al.*, Phys. Rev. B **51**, 14 794 (1995).
[14] L. Gránásy *et al.*, in *Physics and Chemistry of Fullerenes and Derivatives* (World Scientific, Singapore, 1995), p. 331.
[15] J. Winter and H. Kuzmany, Solid State Commun. **84**, 935 (1992).
[16] Q. Zhu, D. E. Cox, and J. E. Fischer, Phys. Rev. B **51**, 3966 (1995).
[17] G. Oszlányi *et al.*, Phys. Rev. B **51**, 12 228 (1995).
[18] M. C. Martin *et al.*, Phys. Rev. B **49**, 10 818 (1994).
[19] S. Stafström, M. Boman, and J. Fagerström, Europhys. Lett. **30**, 295 (1995).
[20] M. J. S. Dewar, E. G. Zoebisch, E. F. Healy, and J. J. P. Stewart, J. Am. Chem. Soc. **107**, 3902 (1985).
[21] J. Ridley and M. Zerner, Theor. Chim. Acta **32**, 111 (1973).
[22] J. A. Pople, D. L. Beveridge, and P. A. Dobosh, J. Chem. Phys. **47**, 2026 (1967).
[23] R. D. Bendale, J. D. Baker, and M. C. Zerner, Int. J. Quantum Chem., Quantum Chem. Symp. **25**, 557 (1991).
[24] Y. Wang, J. M. Holden, X.-x. Bi, and P. C. Eklund, Chem. Phys. Lett. **217**, 413 (1994).
[25] J. Fagerström (unpublished).
[26] J. D. Baker and M. C. Zerner, J. Phys. Chem. **95**, 8614 (1991).
[27] J. Oddershede, P. Jørgensen, and D. L. Yeager, Comput. Phys. Rep. **2**, 33 (1984).
[28] J. Oddershede and J. R. Sabin, Int. J. Quantum Chem. **39**, 371 (1991).
[29] Y. Wang *et al.*, Phys. Rev. B **51**, 4547 (1995).
[30] S. Leach *et al.*, Chem. Phys. **160**, 451 (1992).
[31] J. Fagerström and S. Stafström, Chem. Phys. Lett. **203**, 81 (1993).
[32] C. S. Yannoni *et al.*, J. Phys. Chem. **95**, 9 (1991).